

Wave Propagation in a Randomly Rough Parallel-Plate Waveguide

Ruihua Ding, Leung Tsang, *Fellow, IEEE*, and Henning Braunsch, *Senior Member, IEEE*

Abstract—We study the effects of random rough surface on electromagnetic wave propagation in a parallel-plate waveguide excited by a line source. The second-order small perturbation method is applied to derive a closed-form expression for the coherent wave propagation and the power loss. The derived result is expressed in terms of a double Sommerfeld integral. The double Sommerfeld integral is evaluated by direct numerical integration and by approximate methods. The results of the two methods are shown to be in good agreement with each other. Numerical results of coherent wave propagation and power loss are illustrated as a function of roughness characteristics and waveguide thickness. The enhancement factors are compared with previous results of plane-wave scattering. The waveguide model and the plane-wave model are in good agreement for moderate to large waveguide thicknesses. For small waveguide thickness, the waveguide model shows significantly different power loss as compared to the plane-wave model. Full-wave simulations by the finite-element method are used to validate the second-order small perturbation in waveguide model.

Index Terms—Finite-element method (FEM), perturbation method, rough surface, waveguide, wave propagation.

I. INTRODUCTION

IN HIGH-SPEED interconnects on printed circuit boards (PCBs) and microelectronic packages, the interface between signal traces and substrate is often roughened to improve adhesion. The skin depth of copper becomes comparable to the root mean square (rms) height of the rough surface when frequency is in the gigahertz range. Thus, the signal distortion caused by roughness is not negligible at multigigahertz frequencies. In his classical paper, Morgan [1] studied the power dissipation due to eddy currents in a metallic rough surface at microwave frequencies. In the paper, a 2-D problem is treated and the rough surface is modeled as periodic grooves of various shapes and sizes transverse to the direction of induced current flow. Hammerstad and Bekkadal [2] derived a widely used formula that matches the numerical results of Morgan. The formula in [2] is given as an enhancement factor describing the ratio of the power absorption of rough surface to that of smooth surface.

The rough surface power loss in [2] depends only on the rms height of the rough surface. Other characteristics of the

rough surface such as the slopes of the roughness and the type of rough surface are not included. Holloway and Kuester [3], [4] studied the 2-D power loss of conducting rough interfaces by the generalized impedance boundary condition, where the effective fields outside the conductor can be obtained without knowing the fields inside the conductor. However, the generalized impedance boundary condition is difficult to implement if the roughness has fine scale structures. Proekt and Cangellaris [5] applied perturbation theory to find the ohmic loss caused by a periodically triangle-grooved air-metal interface. Wu [6] analyzed the increase of resistance of rough surface conductors with Morgan's squared-groove periodic structure. Chen [7] modeled the conductor loss in transmission lines using a commercial full-wave solver. The 3-D rough surface was represented by periodic hexagonal pyramidal shapes. Lukic [8] studied the effects of symmetric rectangular, semicircular, and triangular grooves on the propagation constant of transmission lines by the finite-element method (FEM). In these previous studies, surface roughness was characterized by structures of regular shapes or periodic grooves.

Recently, our group [9]–[11] adopted a random rough surface model characterized by correlation function and spectral density instead of considering periodic structures. Typical parameters are rms height, correlation length, and the type of correlation function, e.g., Gaussian or exponential correlation function. In [11] and [12], the spectral densities are extracted from real-life 3-D roughness profiles measured by atomic force microscopy (AFM). The results of roughness effects were first developed by studying the 2-D case using the second-order small perturbation method (SPM) [13], [14] and by numerical methods such as the method of moments [15]. Subsequently, the results were extended to the 3-D case using the second-order SPM and T-matrix method [15]. The enhancement factors are calculated and illustrated as a function of roughness parameters. The advantage of using SPM is that closed-form analytic expressions of the enhancement factor for both 2-D and 3-D cases can be derived [9], [10].

In our previous papers, the problem is modeled as plane-wave scattering and absorption by a random rough surface. However, electromagnetic (EM) waves propagate in a waveguide environment for interconnect problems. Thus, in this paper, the effects of random roughness on wave propagation are studied by a waveguide model. The wave excitation is by a line source in a parallel-plate waveguide. The integral equations are formulated using the half-space Green's function. As in the simpler plane-wave problem, the SPM is applied to solve the integral equation. The results of coherent wave propagation and power absorption along the waveguide are expressed in terms of double

Manuscript received January 30, 2009; revised February 06, 2009. First published April 17, 2009; current version published May 06, 2009. This work was supported by the Intel Corporation.

R. Ding and L. Tsang are with the Department of Electrical Engineering, University of Washington, Seattle, WA 98195 USA (e-mail: dingr@u.washington.edu; tsangl@u.washington.edu).

H. Braunsch is with Components Research, Intel Corporation, Chandler, AZ 85226 USA (e-mail: henning.braunsch@intel.com).

Digital Object Identifier 10.1109/TMTT.2009.2017366

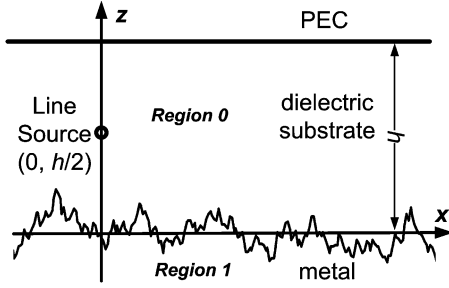


Fig. 1. Waveguide model with random roughness. The waveguide is of thickness h ; a line source is located at $(0, h/2)$.

Sommerfeld integrals, which are solved by direct numerical integration and by approximate methods. The results of the two methods are in good agreement. We illustrate the numerical results of coherent wave propagation as a function of roughness characteristics and as a function of waveguide thickness. The results show that the coherent wave decay of a rough surface waveguide is larger than that of a smooth waveguide. The phase angle of the coherent wave shows that the rough waveguide has more phase shift than a smooth waveguide, corresponding to an expected increase in effective propagation constant. The enhancement factor is defined as the ratio of decay constants. The results for the waveguide model are compared with previous results derived from the plane-wave model. When the waveguide thickness is large, the results of enhancement factor agree with that of the plane-wave case. When the waveguide thickness is small, the enhancement factor of the waveguide model is larger than that of the plane-wave model. Full-wave simulations implemented by the FEM are in agreement with the SPM waveguide model results, showing an increase in enhancement with a decrease of waveguide thickness. The results show that the waveguide thickness effects on the enhancement factor can be nonnegligible when the dielectric thickness is less than $100 \mu\text{m}$ and the surface is very rough.

II. METHOD

A. Line Source Excitation in Parallel-Plate Waveguide

Fig. 1 illustrates the structure of the parallel-plate waveguide with a material of dielectric permittivity ε and wavenumber k (region 0) placed between two conductors. The waveguide is infinitely long in the x - and y -directions. To simplify the problem, we assume that the upper wall at $z = h$ is a perfect electric conductor (PEC) with a smooth surface. The surface between the dielectric and lower metal is rough with the surface height function described by $z = f(x)$. The metal (region 1) is of finite conductivity σ with wavenumber k_1 . The 2-D line source is located at (x_0, z_0) . Let the observation point be at (x, z) .

An also rough top plate can be important for practical rough surface problems. However, using the second-order theory of SPM, the roughness effect is represented by the cross term that is the product of the zeroth- and second-order fields. In the second-order term, the correction is proportional to the height roughness correlation function $\langle f(x)f(x') \rangle$. The random height profile of the bottom plate and that of the top plate are independent, thus $\langle f_{\text{bottom}}(x)f_{\text{top}}(x') \rangle = 0$, which means there is no

interaction between the two height functions in the second-order theory. The roughness effects of the top and bottom plate are then independent. The roughness absorption due to both plates is simply the sum of the two in the second-order theory. Therefore, in this paper, the model is composed of a PEC plane at the top and a bottom finite-conductivity plane with a rough surface.

B. Random Rough Surface Characteristics

The rough surface height function $f(x)$ is assumed to be a statistical homogeneous random process with zero mean and correlation function $C(x)$ such that $\langle f(x_1)f(x_2) \rangle = h_{\text{RMS}}^2 C(|x_1 - x_2|)$. The angular brackets represent the expected value of the random process. Let $F(k_x)$ be the Fourier transform of the height function $f(x)$ with $\langle F(k_x)F(k'_x) \rangle = 4\pi\delta(k_x + k'_x)W(k_x)$. Here, the power spectral density (PSD) $W(k_x)$ is the Fourier transform of the correlation function $C(x)$. The PSD for a Gaussian correlation function is also the Gaussian function $W(k_x) = h_{\text{RMS}}^2 l / 2\sqrt{\pi} \exp(-k_x^2 l^2 / 4)$. The PSD for the exponential correlation function is $W(k) = h_{\text{RMS}}^2 l / (1 + k_x^2 l^2) / \pi$ [13]. The generalized PSD function used to describe surface spectra falling in between Gaussian and exponential PSDs for 1-D rough surfaces is given by [16]

$$W(k) = \frac{h^2 l}{\sqrt{4\pi} b_p} \left[1 + \left(\frac{a_p k l}{b_p} \right)^2 \right]^{-p}, \quad p \geq 1 \quad (1)$$

where $a_p = \Gamma(p - 0.5) / \Gamma(p)$ and b_p satisfies

$$[2b_p / a_p]^{p-0.5} K_{p-0.5}(2b_p / a_p) = 2^{p-1.5} \Gamma(p - 0.5) e^{-1}. \quad (2)$$

$K_{p-0.5}$ is the Bessel function of imaginary argument, and $\Gamma(p)$ denotes the Gamma function with p being the power index.

C. Extinction Theorem and SPM

The wave function ψ can represent the magnetic field along the y -direction. Denote $\psi = H_y$ in region 0 and $\psi = H_{1y}$ in region 1. They satisfy the extinction theorem [13]

$$\psi_{\text{inc}}(\bar{r}) = - \int_{S'} dS' \hat{n}' \cdot [\psi(\bar{r}') \nabla' g_{00}(\bar{r}, \bar{r}') - g_{00}(\bar{r}, \bar{r}') \nabla' \psi(\bar{r}')] \quad \bar{r} \in \text{Region 1} \quad (3)$$

and

$$\int_{S'} dS' \hat{n}' \cdot [\psi_1(\bar{r}') \nabla' g_1(\bar{r}, \bar{r}') - g_1(\bar{r}, \bar{r}') \nabla' \psi_1(\bar{r}')] = 0 \quad \bar{r} \in \text{Region 0}. \quad (4)$$

In these equations, g_{00} is the 2-D half-space Green's function and g_1 is the Green's function in the metallic region [13]. \bar{r} and \bar{r}' denote the observation point and rough surface point S' , respectively. The incident wave function associated with the line source is the 2-D half-space Green's function g_{00} .

On the rough surface, $z' = f(x')$, $\psi(r) = \psi_1(r)$, and $\varepsilon_1 \hat{n} \cdot \nabla \psi(\bar{r}) = \varepsilon \hat{n} \cdot \nabla \psi_1(\bar{r})$, which corresponds to continuity of tangential electric field. To solve the coupled surface integral equations, let $a(x')$ and $b(x')$ denote the surface unknown wave-

function and its normal derivative on the surface as (5) and (6), respectively. Next we apply the second-order SPM [13] to the equations. The two unknowns $a(x')$ and $b(x')$ are expanded to second order as (7)

$$\begin{aligned} \psi(x', f(x')) &= a(x') \\ \sqrt{1 + \left(\frac{df(x')}{dx'}\right)^2} [\hat{n}' \cdot \nabla' \psi(x', f(x'))] & \\ &= b(x') \\ a(x') &= a^{(0)}(x') + a^{(1)}(x') + a^{(2)}(x') \\ b(x') &= b^{(0)}(x') + b^{(1)}(x') + b^{(2)}(x'). \end{aligned} \quad (7)$$

Substituting (7) in (3) and balancing to second order, the solutions of $a(x')$ and $b(x')$ can be found. Once the field on the rough surface $\psi(r')$ is known, the wave function $\psi(r)$ in the waveguide (region 0) can be obtained from the extinction theorem.

III. DERIVATION OF A CLOSED-FORM EXPRESSION FOR THE COHERENT WAVE PROPAGATION AND THE POWER LOSS BASED ON SPM

A. Coherent Wave Propagation Up to Second Order

The expectation value of magnetic field ψ is called the coherent field or the first moment of the field, which can be expressed as follows in (8)–(11) based on the discussion in Section II:

$$\langle \psi(\bar{r}) \rangle = \langle \psi^{(0)}(\bar{r}) \rangle + \langle \psi^{(1)}(\bar{r}) \rangle + \langle \psi^{(2)}(\bar{r}) \rangle \quad (8)$$

$$\begin{aligned} \langle \psi^{(0)}(\bar{r}) \rangle &= \frac{1}{4\pi j} \int_{-\infty}^{\infty} dk_x \frac{1}{k_z Q(k_x)} \exp(-jk_x(x-x_0)) \\ &\times \{ [\exp(jk_z(z-z_0)) + \exp(-jk_z(2h-z-z_0))] \\ &\times [k_z(1-\exp(-jk_z2h)) \\ &\quad + mk_{1z}(1+\exp(-jk_z2h))] \\ &+ [\exp(-jk_zz) + \exp(-jk_z(2h-z))] \\ &\times (k_z - mk_{1z}) \\ &\times [\exp(-jk_zz_0) + \exp(-jk_z(2h-z_0))] \} \end{aligned} \quad (9)$$

$$\langle \psi^{(1)}(\bar{r}) \rangle = 0 \quad (10)$$

$$\begin{aligned} \langle \psi^{(2)}(\bar{r}) \rangle &= \int_{-\infty}^{\infty} dk_x \frac{k_z}{2\pi Q(k_x)} \exp(-jk_x x) \\ &\cdot [\exp(-jk_z z) + \exp(-jk_z(2h-z))] A^{(0)}(k_x) \\ &\times \{ k_x \langle AkF \rangle / k_z + k_{1z} \langle BF \rangle / k_z \\ &\quad + (k_z - mk_{1z}^2 / k_z) \langle AF \rangle \} \end{aligned} \quad (11)$$

where

$$\begin{aligned} \langle AF \rangle &= \int_{-\infty}^{\infty} dk'_x \frac{W(k'_x - k_x)}{Q(k'_x)} \\ &\times [(1 + \exp(-jk_z2h)) \\ &\quad \times (-mk'_x k_x + k'_x k_x - mk'_{1z} k_{1z}) \\ &\quad - (1 - \exp(-jk_z2h)) mk_{1z} k'_z] \end{aligned} \quad (12)$$

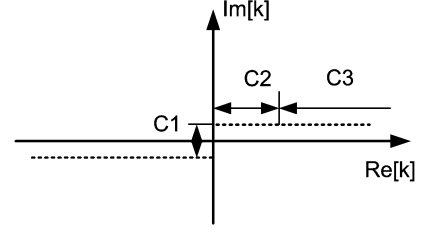


Fig. 2. Sommerfeld integration contour.

$$\begin{aligned} \langle AkF \rangle &= \int_{-\infty}^{\infty} dk'_x \frac{(k'_x - k_x) W(k'_x - k_x)}{Q(k'_x)} \\ &\times [(\exp(-jk_z2h) - 1) mk_{1z} k'_z \\ &\quad + (1 + \exp(-jk_z2h)) \\ &\quad \times (-mk'_x k_x + k'_x k_x - mk'_{1z} k_{1z})] \end{aligned} \quad (13)$$

$$\begin{aligned} \langle BF \rangle &= \int_{-\infty}^{\infty} dk'_x \frac{1}{Q(k'_x)} m W(k'_x - k_x) \\ &\times [(1 + \exp(-jk_z2h)) k'_{1z} (-k^2 + k'_x k_x) \\ &\quad + (1 - \exp(-jk_z2h)) k'_z \\ &\quad \times (-k_1^2 + k'_x k_x - mk'_{1z} k_{1z} + k'_{1z} k_{1z})] \end{aligned} \quad (14)$$

$$\begin{aligned} A^{(0)}(k_x) &= \frac{\exp(jk_x x_0) [\exp(-jk_z z_0) + \exp(-jk_z(2h-z_0))]}{jQ(k_x)} \\ Q(k_x) &= k_z (1 - \exp(-jk_z2h)) + mk_{1z} (1 + \exp(-jk_z2h)) \\ m &= \varepsilon / \varepsilon_1. \end{aligned} \quad (15)$$

The zeroth-order coherent field can be obtained from (9) by applying residue calculus. For interconnect problems, h is much less than the wavelength so that there is only one propagating mode; all other modes are cut off and decay exponentially. Thus, when x is at more than several h from the source at x_0 , the cutoff modes are negligible. The first-order coherent field is zero.

The second-order solution of the coherent field is (11). We observe that $\langle \psi^{(2)}(\bar{r}) \rangle$ consists of a double Sommerfeld integral $\int_C dk_x \int_C dk'_x$, where C is the Sommerfeld integration path (SIP) shown in Fig. 2. The inner integral $\int_0^\infty dk'_x$ is given in (12)–(14). The outer integral $\int_0^\infty dk_x$ is given in (11).

B. Direct Numerical Integration of Double Sommerfeld Integral

The Sommerfeld integral can be decomposed into three parts, i.e., C_1 , C_2 , and C_3 , as shown in Fig. 2 for $k_x > 0$. The analysis for the integral contour with $k_x < 0$ is similar as above.

a) Inner Integral: $\int_0^\infty dk'_x$ Integration:

1. C_1 is along the imaginary k'_x axis so that $k'_x = ik'_{xi}$ and k'_{xi} is from 0 to $k'_{xi\max}$. In this way, the integral contour has no pole singularities. We choose the upper limit of the contour as $k'_{xi\max} = \min(0.03/l, 0.01k)$ and the sampling $\Delta k'_{xi} = \min(0.3k'_{xi\max}, 0.2/h)$.
2. C_2 is parallel to the real k'_x axis from 0 to $k'_{xr1\max}$. The imaginary part is fixed at $k'_{xi\max}$ and the real part varies from 0 to $k'_{xr1\max}$, i.e., $k'_x = k'_{xr} + ik'_{xi\max}$. We choose $k'_{xr1\max} = 10k$. Since the waveguide poles are close to C_2 , we choose a fine sampling interval of $\Delta k'_{xr1} = \Delta k'_{xi}$.

3. C_3 is parallel to the real k'_x axis from $k'_{xr1\max}$ to $k'_{xr2\max}$. The imaginary part is fixed at $k'_{xi\max}$. Thus, $k'_x = k'_{xr} + ik'_{xi\max}$. We set $k'_{xr1\max} = 10/l$. Along the SIP of C_3 , k'_x is far away from the waveguide poles. Therefore, k'_x , the sampling, can be coarse and is set to $\Delta k'_{xr2} = \min(0.05k_1, 1/20l)$.

b) *Outer Integral*: $\int_0^\infty dk_x$ *Integration*: On completion of the inner integral, there is no dependence on the rough surface correlation length for the outer integral. Thus, the choices in numerical integration are different from the case of the inner integral.

1. C_1 is along the imaginary k_x axis. $k_x = ik_{xi}$ and k_{xi} are from 0 to $k_{xi\max}$. $k_{xi\max} = \min(0.03/x, 0.002k)$. The sampling step is $\Delta k_{xi} = 0.3k_{xi\max}$.
2. C_2 is parallel to the real axis. Along C_2 , $k_x = k_{xr} + ik_{xi\max}$. k_{xr} varies from 0 to $k_{xr1\max}$. $k_{xr1\max} = 10k$ and $\Delta k_{xr1} = 0.3k_{xi\max}$.
3. C_3 is parallel to the real axis. Along C_3 , $k_x = k_{xr} + ik_{xi\max}$. The imaginary part is still $k_{xi\max}$ and the real part is from $k_{xr1\max}$ to $k_{xr2\max}$. $k_{xr2\max} = \max(10k, 5/h)$. Along the SIP of C_3 , k_x is far away from the waveguide poles. Therefore, the sampling step can be larger and we choose $\Delta k_{xr2} = 7k_{xi\max}$.

Evaluation of the double Sommerfeld integral by the direct method is time consuming and requires several CPU hours for each observation point. Thus, we have developed an approximate method for evaluation of the double Sommerfeld integral. The approximation is based on the property that the correlation length is on the order of micrometers, while the wavenumber in the dielectric is on the order of cm^{-1} . Thus, $kl \ll 1$ and is on the order of 10^{-4} .

C. Approximate Integration Method of Double Sommerfeld Integral

a) *Inner Integral*: $\int_0^\infty dk'_x$ *Integration*:

1. Along C_1 : $k'_x = ik'_{xi}$ since $k'_{xr\max} \gg k'_{xi\max}$. The integral along the path C_1 is negligible compared with the one along C_2 and can be ignored for the inner integral.
2. Along C_2 : the correlation length l of the rough surface is on the order of micrometers. The wavenumber of the substrate is on the order of 10^3 m^{-1} . Thus, we have the relation $k'_{xr1\max} \ll k'_{xr2\max}$ and the integral along C_2 can be ignored.
3. Along C_3 : this can be approximated by integrating from $k'_{xr1\max} = 10k$ to $k'_{xr2\max} = 10/l$. In this region, $k'_{xr} \gg k$. Thus, for the inner integral, only C_3 remains.

b) *Outer Integral*: $\int_0^\infty dk_x$ *Integration*:

1. C_1 : the integral along C_1 can be ignored for the same reason as for the inner integral.
2. C_2 : the integral along C_2 is the main contribution for the outer integral.
3. C_3 : the integrand decreases rapidly with k_{xr} . Therefore, the integral along C_3 can be ignored. Thus, for the outer integral, only C_2 remains and k_x is on the order of k .

c) *Approximated Closed-Form Integral*: Thus, the inner integral is only over C_3 and the outer integral is only along C_2 . In these respective regions, we can approximate the integrand further. The permittivity ε of the dielectric is much smaller than

that of metal ε_1 , i.e., $k_1 \gg k$. On contour, $C_3 k \ll k'_x$. On contour, $C_2 k_1 \gg k_x$. Under these approximations, (11) can be simplified to

$$\begin{aligned} \langle \psi^{(2)}(\bar{r}) \rangle &= \frac{j}{2\pi} \int_{-\infty}^{\infty} dk_x \frac{\exp(-jk_x(x-x_0))}{[Q(k_x)]^2} \\ &\cdot [\exp(-jk_z z) + \exp(-jk_z(2h-z))] \\ &\cdot [\exp(-jk_z z_0) + \exp(-jk_z(2h-z_0))] \\ &\cdot \left[k^2 \left(k_{1z} h_{\text{RMS}}^2 - \int_{-\infty}^{\infty} dk'_x W(k'_x) k'_{1z} \right) \right. \\ &\quad \left. + k_x^2 \int_{-\infty}^{\infty} dk'_x W(k'_x) \frac{k_x^{2l}}{k'_z} \right]. \end{aligned} \quad (16)$$

For the inner integral, we extend from 0 to infinity for C_3 because sampling needs to be on the order of the inverse of the correlation length of the rough surface. The integral of $\langle \psi^{(0)} \rangle$ in (9) and $\langle \psi^{(2)} \rangle$ in (11) have the same poles. A major difference is that for $\langle \psi^{(0)} \rangle$, the poles are of first order, while for $\langle \psi^{(2)} \rangle$, the poles are of second order. After obtaining the integrals of $\int_{-\infty}^{\infty} dk'_x W(k'_x) k'_{1z}$ and $\int_{-\infty}^{\infty} dk'_x W(k'_x) k_x^{2l}/k'_z$, the outer integral in $\langle \psi^{(2)} \rangle$ can be calculated by residue theory for second-order poles. The approximate method requires CPU time of only seconds per observation point.

D. Coherent Wave and Cascading

The second-order term $\psi^{(2)}$ grows with propagation distance x , typically for small perturbation theory. To improve the solution, we use the method of cascading, as discussed in [14]. Divide x into n small sections of separation x/n . If n is large, then the distance x/n is small enough so that the SPM applies. The coherent wave after distance x/n becomes (17). After a total distance x , the result is that of cascading n times the above effect of distance x/n . The coherent wave at x can be expressed as (18), which does not grow with propagation distance x

$$\left\langle \psi \left(\frac{x}{n} \right) \right\rangle = \langle \psi^{(0)} \rangle \left(1 + \frac{\langle \psi^{(2)} \rangle}{n \langle \psi^{(0)} \rangle} \right) \quad (17)$$

$$\begin{aligned} \langle \psi(x) \rangle &= \lim_{n \rightarrow \infty} \langle \psi^{(0)} \rangle \left[1 + \frac{\langle \psi^{(2)} \rangle}{n \langle \psi^{(0)} \rangle} \right]^n \\ &= \langle \psi^{(0)} \rangle \exp \left(\frac{\langle \psi^{(2)} \rangle}{\langle \psi^{(0)} \rangle} \right). \end{aligned} \quad (18)$$

E. Poynting Vector of Coherent Wave Up to Second Order

Given the coherent wave in the waveguide, the Poynting vector of the coherent wave $\langle S \rangle_{\text{coh}}$ along the guidance direction x can be calculated. The zeroth order is the Poynting vector for the smooth-surface waveguide and is given by

$$\langle \bar{S} \cdot \hat{x} \rangle_{\text{smooth}} = \text{Re} \left\{ \frac{j}{2\omega\varepsilon} \langle \psi^{(0)}(\bar{r}) \rangle \left\langle \frac{\partial}{\partial x} \psi^{(0)*}(\bar{r}) \right\rangle \right\}. \quad (19)$$

TABLE I
COMPARISON BETWEEN DIRECT AND APPROXIMATE METHOD

Waveguide thickness h (μm)	CPU time per point: Direct method	CPU time per point: Approximate method	Relative error b/w (11) and (16)
100	3 hrs	0.11 s	0.01%
50	5 hrs	0.11 s	0.09%
25	13.5 hrs	0.11 s	0.5%
10	91 hrs	0.12 s	3.25%

The wave function ψ and its derivative for the rough surface waveguide are obtained as (8). The Poynting vector of the coherent wave up to the second order for the rough surface waveguide is

$$\langle \vec{S} \cdot \hat{x} \rangle_{\text{coh,rough}} = \text{Re} \left\{ \frac{j}{2\omega\epsilon} \langle \psi \rangle \left\langle \frac{\partial \psi^*}{\partial x} \right\rangle \right\}. \quad (20)$$

where the superscript * denotes complex conjugation.

The integrals involved in Poynting vector (20) are $\int_{-\infty}^{\infty} dk'_x \text{Re}[W(k'_x)k'_{1z}]$ and $\int_{-\infty}^{\infty} dk'_x \text{Re}[W(k'_x)k'_x k'_{1z}]/k'_z$, which are convergent for all spectral densities.

IV. RESULTS AND DISCUSSION

A. Parameters in the Model

In the following numerical simulation, the complex permittivity of the dielectric medium is $\epsilon = 3.4\epsilon_0$. When the frequency is 10 GHz, the wavelength in the dielectric substrate is 1.626 cm. The conductivity for the ground plane is assumed to be $\sigma = 5.8 \times 10^7$ S/m. The unit line source is located at the center of the waveguide $(x_0, z_0) = (0, h/2)$. The observation points are located at the center line of the waveguide at $(x, h/2)$.

B. Comparisons Between Direct Numerical Integration and Approximate Numerical Integration

In Table I, we compare CPU time and accuracy between the direct numerical integration method and the approximate numerical integration method for various waveguide thicknesses, assuming a Gaussian spectral density function. The rms height is $h_{\text{RMS}} = 1.5 \mu\text{m}$ and the correlation length $l = 3 \mu\text{m}$. The field observation point is located at a distance of three times the wavelength from the source point, which is 24 mm at 20 GHz. The computational speedup achieved by the approximate method is three to four orders of magnitude. The relative errors are small, except for the small thickness case of $h = 10 \mu\text{m}$. In the approximate method, the upper limit of the outer integral in (11) is related to $5/h$. When h decreases, $k_{x\text{rmax}}$ increases and the approximation $k_1 \gg k_x$ no longer holds. For the remaining results of this section, the waveguide thicknesses are chosen to be $25 \mu\text{m}$ or above, applicable to most on-package and on-board interconnect problems.

C. Coherent Wave and Poynting Vector

In this section, the coherent wave propagation will be discussed using the results of the cascade method in conjunction with the second-order SPM solution.

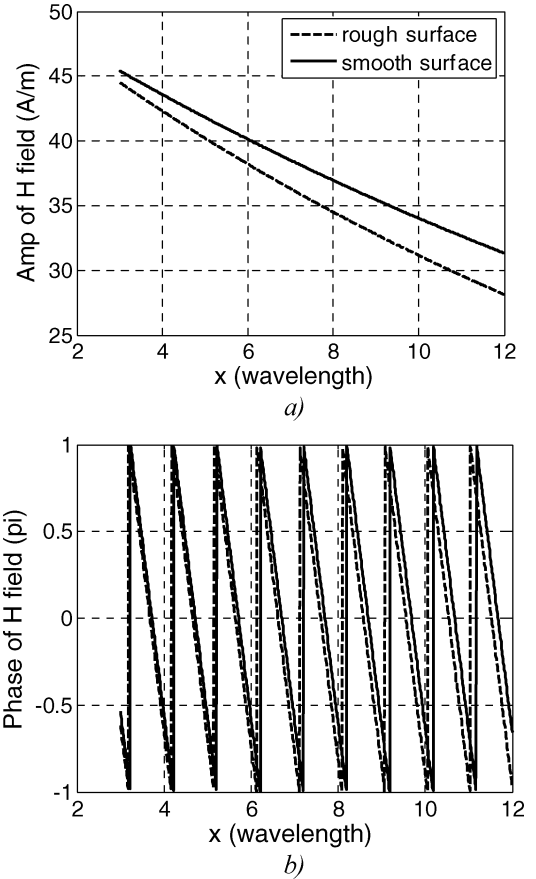


Fig. 3. Amplitude and phase of the H -field in the waveguide at a distance of 2–12 wavelengths for both smooth waveguide (solid line) and rough waveguide (dashed line). The rms height of the Gaussian rough surface is $1 \mu\text{m}$ and the correlation length is $2 \mu\text{m}$. (a) Amplitude of H field. (b) Phase of H -field.

Fig. 3 shows the amplitude and phase angle comparison between the H field of smooth surface waveguide and rough surface waveguide. The correlation function of the rough surface is Gaussian with rms height $h_{\text{RMS}} = 1 \mu\text{m}$ and correlation length $l = 2 \mu\text{m}$. The waveguide thickness is $h = 25 \mu\text{m}$ and the frequency is 10 GHz.

The results show that the coherent wave decay with distance for the rough waveguide is larger than for a smooth waveguide. The phase angle of the coherent wave shows that the rough waveguide exhibits more phase shift than a smooth waveguide corresponding to an increase in phase constant or slow down in phase velocity.

Fig. 4 shows the Poynting vector of the coherent wave of the same simulation model. The Poynting vector can be approximated as an exponential function of the distance between the source and observation point. The distance is displayed up to 30 wavelengths to show the exponential trend.

D. Roughness Absorption Enhancement Factor

The basic idea of absorption enhancement factor is comparing the absorption for a rough surface to a corresponding smooth surface made of the same material. In the transmission line, the propagating wave can be approximated as quasi-TEM

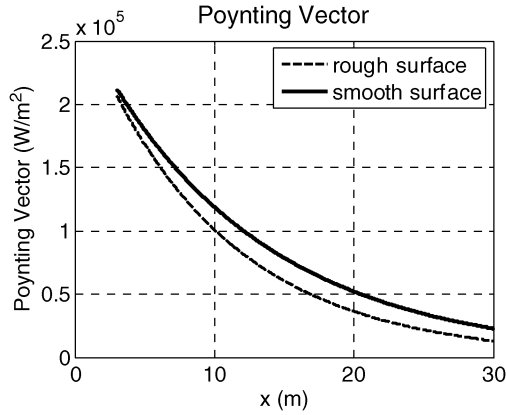


Fig. 4. Poynting vector propagated along the waveguide at a distance up to 30 wavelengths for a smooth waveguide (solid line) and rough waveguide (dashed line). The rms height of the Gaussian rough surface is $1 \mu\text{m}$ and the correlation length is $2 \mu\text{m}$.

mode at a distance of $5h$ away from the source, where all cutoff modes have vanished. Hence, we assume that the wave decays exponentially, which is also shown in Fig. 4. Based on the assumption, the absorption enhancement factor E_w can be defined as the exponential decay constant (or attenuation constant) ratio

$$E_w = \frac{\alpha_{\text{rough}}}{\alpha_{\text{smooth}}} = \frac{\log(\langle \vec{S} \cdot \hat{x} \rangle_{\text{rough}}|_{x=x_1} / \langle \vec{S} \cdot \hat{x} \rangle_{\text{rough}}|_{x=x_2})}{\log(\langle \vec{S} \cdot \hat{x} \rangle_{\text{smooth}}|_{x=x_1} / \langle \vec{S} \cdot \hat{x} \rangle_{\text{smooth}}|_{x=x_2})} \quad (21)$$

where α_{rough} is the exponential decay constant for the rough surface waveguide and α_{smooth} is for the smooth surface waveguide. x_1 and x_2 should be larger than 10^{-3} wavelengths because in the case of interconnects, $5h$ is only approximately 10^{-3} wavelengths.

Having identified the definition of enhancement factor in the waveguide case, we now study the enhancement factor for different rough surface waveguides and compare them with the ones obtained from the plane-wave model [9]. In the previous plane-wave model, the enhancement factor E_p is given by [9]

$$E_p = 1 + \frac{2h_{\text{RMS}}^2}{\delta^2} - \frac{4}{\delta} \int_0^\infty dk_x \text{Re} \left[W(k_x) \sqrt{-\frac{2j}{\delta^2} - k_x^2} \right]. \quad (22)$$

Figs. 5 and 6 compare the results from the plane-wave model and waveguide model for rms height h_{RMS} varying from 0.2 to $1.5 \mu\text{m}$ with correlation length $l = 2 \mu\text{m}$. The waveguide thicknesses are $h = 200 \mu\text{m}$ in Fig. 5 and $h = 25 \mu\text{m}$ in Fig. 6. Cases of Gaussian and exponential correlation functions are shown. The operating frequency varies from 1 to 20 GHz.

For $h = 200 \mu\text{m}$, Fig. 5(a) shows that, for the case of a Gaussian correlation function, the enhancement factor of the waveguide model is the same as that of the plane-wave model. This shows that, for appreciable waveguide thickness and for the Gaussian correlation function, the roughness effect on the quasi-TEM mode can be approximated by that of a plane wave. However, for the case of an exponential correlation function,

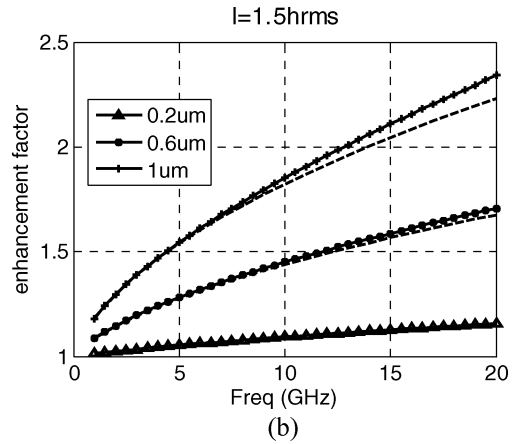
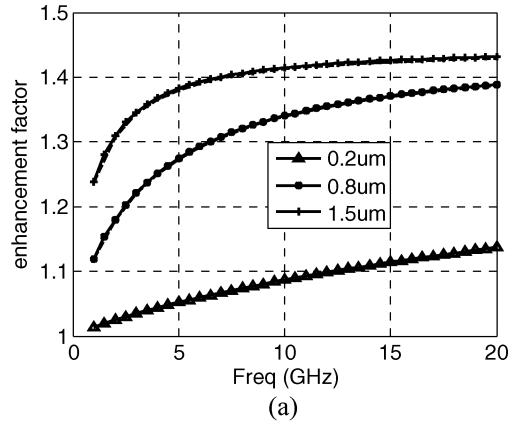


Fig. 5. Enhancement factor comparison of plane-wave model and waveguide model. Waveguide thickness $h = 200 \mu\text{m}$. The triangle, asterisk (*), and cross (+) show the enhancement factor for different h_{RMS} . The dashed line is the enhancement factor of the plane wave with the corresponding h_{RMS} . (a) Gaussian rough surface with $h_{\text{RMS}} = 0.2, 0.8,$ and $1.5 \mu\text{m}$ and $l = 1.5 h_{\text{RMS}}$. (b) Exponential rough surface with $h_{\text{RMS}} = 0.2, 0.6,$ and $1 \mu\text{m}$ and $l = 1.5 h_{\text{RMS}}$.

there is a difference for a large rms height of $1 \mu\text{m}$ with the waveguide model having a larger enhancement factor than the plane-wave model. For the case of waveguide thickness of $h = 25 \mu\text{m}$, the difference between the waveguide model and the plane-wave model is more significant, especially for the large roughness case. For example, for an exponential correlation function with $h_{\text{RMS}} = 1 \mu\text{m}$, the difference can be as large as 7% between the waveguide model and plane-wave model at a frequency of 20 GHz. When the roughness of the surface increases, the enhancement factor becomes larger. Both the plane-wave model and the waveguide model demonstrate this trend. Comparing with the plane-wave model, the waveguide model gives a larger enhancement factor at frequencies higher than 10 GHz and for moderate to large roughness.

In the waveguide model, the waveguide thickness h can have a significant influence on the roughness effect. When the waveguide thickness is small, the interaction of the roughness with the propagating EM wave increases, giving a larger roughness effect. The non-TEM character of the lossy waveguide also becomes more pronounced, making the waveguide problem distinctly different from the plane-wave model. By doing numerical testing, we found that when the random rough surface is Gaussian and the waveguide thickness is 40 times larger than

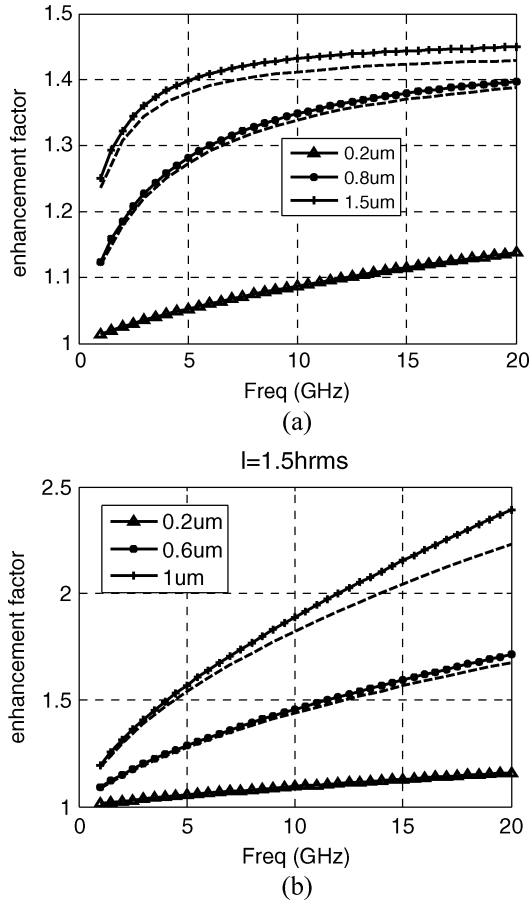


Fig. 6. Enhancement factor comparison of plane-wave model and waveguide model. Waveguide thickness $h = 25 \mu m$. The triangle, asterisk (*), and cross (+) show the enhancement factor for different h_{RMS} . The dashed line is the enhancement factor of the plane wave with the corresponding h_{RMS} . (a) Gaussian rough surface with $h_{RMS} = 0.2, 0.8,$ and $1.5 \mu m$ and $l = 1.5 h_{RMS}$. (b) Exponential rough surface with $h_{RMS} = 0.2, 0.6,$ and $1 \mu m$ and $l = 1.5 h_{RMS}$.

the rms height, the waveguide thickness effect on the enhancement factor is negligible. In this case, the waveguide model and plane-wave model give approximately the same result. When the random rough surface correlation function is exponential, the spectral density function decreases slowly with k_x . This means high spatial spectral components affect the results. Thus, we see that there is a waveguide effect even when the waveguide thickness is 40 times the rms height. Full-wave simulation is performed in Section IV-E to prove this conclusion.

E. Full-Wave Simulation Based on FEM

The waveguide mode-matching technique is applied for full-wave simulation of the power absorbed by the rough surface. Fig. 7 shows the parallel-plate waveguide model excited by a line source. The waveguide structure is divided into regions L , R , and C . In these three regions, the top plate is a smooth PEC plate. The bottom plate is smooth for regions L and R and is rough for region C . The line source lies in region L .

In regions L and R , the structure is simply a parallel-plate waveguide. The field in region L is composed of the incident wave from the line source and the reflected wave from rough surface region C . The field in region R is the transmitted field

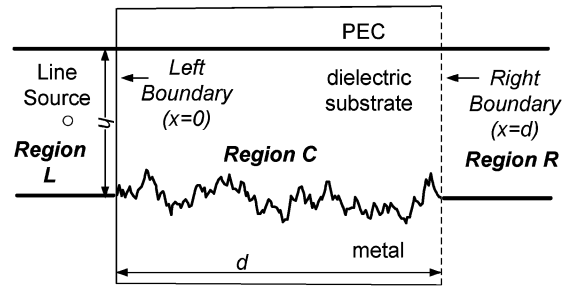


Fig. 7. Full-wave simulation modeling configuration. The dashed line rectangle indicates region C where FEM meshing and calculation are implemented.

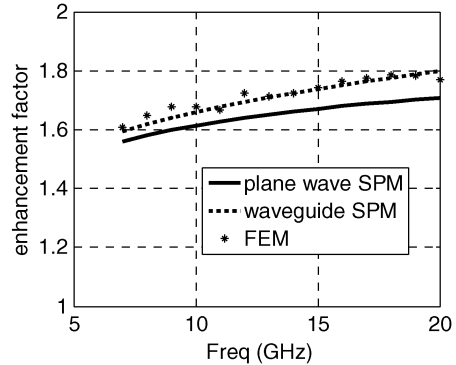


Fig. 8. Numerical simulation result by FEM, compared with SPM of plane-wave model and waveguide model.

from region C . The fields in regions L and C are expressed as summation of waveguide modes. For region C , the FEM is used to construct various solutions. These solutions are then matched to regions L and R through boundary conditions at the junction planes located at $x = 0$ and $x = l$.

Fig. 8 shows the enhancement factor calculated by FEM rough waveguide simulation, SPM of the plane-wave model, and SPM of the waveguide model. The enhancement factors are shown as a function of frequency. For the rough surface, we used a generalized PSD with $p = 2$. The rms height is $1.5 \mu m$ and the correlation length is $2.25 \mu m$. The FEM simulations are in good agreement with the SPM waveguide model, confirming the increase of enhancement in a waveguide relative to that of a plane wave.

In this paper, the rough surface is modeled as a random process. The rms height h_{RMS} and the PSD function are extracted from realizations of the random process for engineering problems. These extracted parameters will have statistical errors, which have been discussed in [11] and [12]. We use an analytical theory of SPM to derive the power absorption, which corresponds to the second moment of the field. To calculate the statistical fluctuations of power absorption requires the calculation of the fourth moment of the field, which is not done for the SPM result in this paper. In the full-wave numerical simulation, Monte Carlo simulations were performed using an FEM based on a periodic boundary condition. The simulations show that using a period of 20 correlation lengths for the case of rms height of $1 \mu m$ and correlation length of $1.5 \mu m$ of the fluctuations of the power absorption are approximately 1.4% at 1 GHz.

V. CONCLUSION

In this paper, we have studied the roughness effects of wave propagation in a parallel-plate waveguide excited by a line source. Applying the SPM, we obtain the closed-form expressions for the coherent wave propagation and the enhancement factor, which was validated by tailored FEM numerical simulation.

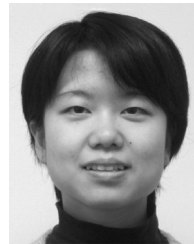
The substrate thickness affects the enhancement factor, defined as the decay constant ratio. The enhancement factors obtained from the plane-wave and waveguide models agree with each other when the thickness is larger than 100 μm . As the thickness decreases, the waveguide enhancement factor is larger than the one obtained from the plane-wave model. The difference increases with surface roughness and with frequency. This conclusion is based on analytical and full-wave numerical simulation (SPM and FEM, respectively).

ACKNOWLEDGMENT

The authors would like to thank X. Gu, IBM T. J. Watson Research Center, Yorktown Heights, NY, and Z. Zhang, Intel Corporation, Chandler, AZ, for useful discussions.

REFERENCES

- [1] S. P. Morgan, Jr., "Effects of surface roughness on eddy current losses at microwave frequencies," *J. Appl. Phys.*, vol. 20, pp. 352–362, Apr. 1949.
- [2] E. O. Hammerstad and F. Bekkadal, "Microstrip handbook," Univ. Trondheim, Trondheim, Norway, ELAB Rep., 1975, pp. 4–8.
- [3] C. L. Holloway and E. F. Kuester, "Power loss associated with conducting and superconducting rough interfaces," *IEEE Trans. Microw. Theory Tech.*, vol. 48, no. 10, pp. 1601–1610, Oct. 2000.
- [4] C. L. Holloway and E. F. Kuester, "Impedance-type boundary conditions for a periodic interface between a dielectric and a highly conducting medium," *IEEE Trans. Antennas Propag.*, vol. 48, no. 10, pp. 1660–1672, Oct. 2000.
- [5] L. Proekt and A. C. Cangellaris, "Investigation of the impact of conductor surface roughness on interconnect frequency-dependent ohmic loss," in *Proc. IEEE Electron. Compon. Technol. Conf.*, New Orleans, LA, May 27–30, 2003, pp. 1004–1010.
- [6] Z. Wu and L. E. Davis, "Surface roughness effect on surface impedance of superconductors," *J. Appl. Phys.*, vol. 76, no. 6, pp. 3669–3672, Sep. 1994.
- [7] X. Chen, "EM modeling of microstrip conductor losses including surface roughness effect," *IEEE Microw. Wireless Compon. Lett.*, vol. 17, no. 2, pp. 94–96, Feb. 2007.
- [8] M. Lukic, "Modeling of 3-D surface roughness effects with application to coaxial lines," *IEEE Trans. Microw. Theory Tech.*, vol. 55, no. 3, pp. 518–525, Mar. 2007.
- [9] L. Tsang, X. Gu, and H. Braunsch, "Effects of random rough surface on absorption by conductors at microwave frequencies," *IEEE Microw. Wireless Compon. Lett.*, vol. 16, no. 4, pp. 221–223, Apr. 2006.
- [10] X. Gu, L. Tsang, and H. Braunsch, "Modeling effects of random rough interface in power absorption between dielectric and conductive medium in 3-D problem," *IEEE Trans. Microw. Theory Tech.*, vol. 55, no. 3, pp. 511–516, Mar. 2007.
- [11] X. Gu, L. Tsang, and H. Braunsch, "Estimation of roughness-induced power absorption from measured surface profile data," *IEEE Microw. Wireless Compon. Lett.*, vol. 17, no. 7, pp. 486–488, Jul. 2007.
- [12] H. Braunsch, X. Gu, A. Camacho-Bragado, and L. Tsang, "Off-chip rough-metal-surface propagation loss modeling and correlation with measurements," in *Proc. IEEE Electron. Compon. Technol. Conf.*, Reno, NV, May 29–Jun. 1, 2007, pp. 785–791.
- [13] L. Tsang, J. A. Kong, and K.-H. Ding, *Scattering of Electromagnetic Waves*. New York: Wiley, 2000, vol. 1, Theory Appl., ch. 9, pp. 397–407.
- [14] L. Tsang and J. A. Kong, *Scattering of Electromagnetic Waves*. New York: Wiley, 2001, vol. 3, Adv. Topics, ch. 1, pp. 2–11.
- [15] L. Tsang, J. A. Kong, K.-H. Ding, and C. O. Ao, *Scattering of Electromagnetic Waves*. New York: Wiley, 2000, vol. 2, Numer. Simulation, ch. 3, pp. 114–118.
- [16] Q. Li and J. Shi, "A generalized power law spectrum and its applications to the backscattering of soil surfaces based on the integral equation model," *IEEE Trans. Geosc. Remote Sens.*, vol. 40, no. 2, pp. 271–280, Feb. 2002.



Ruihua Ding received the M.S. degree from Michigan State University, Lansing, in 2006, and is currently working toward the Ph.D. degree at the University of Washington, Seattle.

Her research interests include characterization of high-speed interconnect and microelectronic packaging, signal and power integrity, and computational electromagnetics.



Leung Tsang (S'73–M'75–SM'85–F'90) received the S.B., S.M., and Ph.D. degrees from the Massachusetts Institute of Technology (MIT), Cambridge.

He is currently a Professor and Chair with the Department of Electrical Engineering, University of Washington, Seattle. He coauthored *Theory of Microwave Remote Sensing and Scattering of Electromagnetic Waves, Vol. 1* (Wiley Intersci., 2000), *Theory of Microwave Remote Sensing and Scattering of Electromagnetic Waves, Vol. 2* (Wiley Intersci., 2001), and *Theory of Microwave Remote Sensing and Scattering of Electromagnetic Waves, Vol. 3* (Wiley Intersci., 2001). His current research interests include remote sensing, signal integrity of interconnects, computational electromagnetics, and wireless communications.

Dr. Tsang was the editor-in-chief of the IEEE TRANSACTIONS ON GEOSCIENCE AND REMOTE SENSING. He is a Fellow of the Optical Society of America (OSA)



Henning Braunsch (S'99–M'01–SM'06) received the M.S. degree in electrical engineering from Michigan State University, East Lansing, in 1995, the M.S. degree in electrical engineering from the University of Hanover, Hanover, Germany, in 1996, and the Ph.D. degree in electrical engineering and computer science from the Massachusetts Institute of Technology (MIT), Cambridge, in 2001.

He is currently with Components Research, Intel Corporation, Chandler, AZ. His research interests and expertise are in advanced microelectronic packaging, applied electromagnetics, physics-based signal processing, and forward and inverse modeling.